

# Weighing the Axion with Muon Haloscopy

N. Bray-Ali\*

*Department of Physical Sciences  
Mount Saint Mary's University  
12001 Chalon Rd.*

*Los Angeles, CA 90049  
(Dated: June 17, 2022)*

Axions in the local dark matter halo of the galaxy collide with virtual photons dressing the electromagnetic vertex of the muon. The collisions shift the muon magnetic moment in a way that scales with the volume of the muon beam and transforms like the axion under the charge conjugation, parity, and time-reversal symmetries of electromagnetism. Analysis of measurements of the muon magnetic moment suggests that axions saturate the local halo energy density and that the axion shift resolves the tension between the measurements and the Standard Model of particle physics. The precision of the mass of the axion determined by muon haloscopy can be improved by a factor of a hundred using Fourier transform infrared spectroscopy of ferroelectric antiferromagnets and by a factor of a million using optical magnetometry of alkali vapor cells illuminated by a cavity-locked infrared laser.

The spin of the muon precesses in a magnetic field  $B$  at frequency  $\omega_a = a_\mu(e/m_\mu)B$ , where,  $a_\mu \approx \alpha/(2\pi) \approx 1.16 \times 10^{-3}$ , and  $e/m_\mu = 2\pi \times 135$  MHz/T is the charge to mass ratio of the muon [1–3]. Compared with the electron, the muon is  $(m_\mu/m_e)^2 \approx 43,000$  times more sensitive to the hadronic leading order contribution  $a_\mu^{\text{HLO}}$  to spin precession [4, 5]. In this Letter, we show that axions in the local dark matter halo of the galaxy shift  $a_\mu$  from the standard model values in a way that scales with the volume of the “haloscope” and that transforms like the axion under the charge conjugation  $C$ , parity  $P$ , and time-reversal  $T$  symmetries of electromagnetism[6].

We start by expressing the axion  $A_M$  in terms of quarks and leptons  $M_H^P$  with helicity  $H = L, R$  and charge-parity check  $P = +, -$  [7]:

$$A_M = M_L^- \overline{M_R^-} - M_R^- \overline{M_L^-} - M_L^+ \overline{M_R^+} + M_R^+ \overline{M_L^+} \quad (1)$$

Here,  $M$  runs over the twelve known “flavors” of quarks and leptons while the charge-parity check  $P$  is  $+$  for quarks and leptons that do not feel the weak nuclear force and  $-$  for those that do. In the standard model, we find  $M_L^-$  and  $M_R^+$ , but neither  $M_L^+$  nor  $M_R^-$ , where,  $L$  is for left-handed and  $R$  is for right-handed helicity [8].

Next, we suppose that axions  $A_M$  of each kind and photons  $\gamma_H$  of each helicity formed in equal numbers in the early universe prior to baryogenesis. This fixes the ratio  $n_A/n_\gamma = |M|/|H| = 6$  of axions to photons and gives the axion mass  $m_A$  ( $\hbar = c = 1$ ) [9]:

$$m_A = 2.70 \text{ k}T_\gamma \left( \frac{n_A}{n_\gamma} \right)^{-1} \frac{\Omega_A h^2}{\Omega_\gamma h^2} = (0.508 \pm 0.004) \text{ eV}, \quad (2)$$

where,  $T_\gamma = (2.7255 \pm 0.0006) \text{ K}$  is the present photon temperature[10],  $\Omega_\gamma h^2 = 2.473 \times 10^{-5}$  is the photon energy density parameter and  $\Omega_A h^2 = 0.11882 \pm 0.0086$  is that of the axions assuming they saturate the dark matter [11].

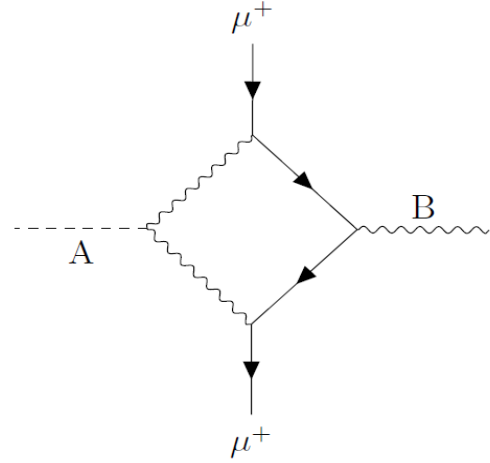


FIG. 1. **Principle of Muon Haloscopy** Halo axion  $A$  collides with virtual photon dressing vertex of positive muon  $\mu^+$  and magnetic field  $B$ .

Figure 1 shows how axions in the local halo shift muon spin precession [1–3]. Acting as a background field  $\tilde{\phi}_A(q_A)$  with on-shell four-momentum  $q_A^2 = m_A^2 \ll m_\mu^2$ , the axion  $A$  couples to the virtual photon dressing the vertex of the positive muon  $\mu^+$  and the magnetic field  $B$ . The shift of the spin precession frequency  $\Delta a_\mu$  grows with the axion-photon coupling  $g_{A\gamma\gamma}$ [12]:

$$\frac{\Delta a_\mu}{a_\mu} = m_A^2 g_{A\gamma\gamma} \tilde{\phi}_A(q_A) = \pm m_A g_{A\gamma\gamma} \sqrt{\rho_A N V T} \quad (3)$$

where, the axion field strength  $|\tilde{\phi}_A(q_A)|^2 \approx \phi_A^2 N V T$  is fixed by the axion energy density  $\rho_A = \phi_A^2 m_A^2$ , the volume  $V$  of the muon beam, the lifetime  $T$  of the muon in the axion rest-frame, and the average number of muons  $N$  during spin precession. The sign of the shift  $\Delta a_\mu$  in Eq. (3) switches along with the axion field  $\tilde{\phi}_A(q_A)$  under

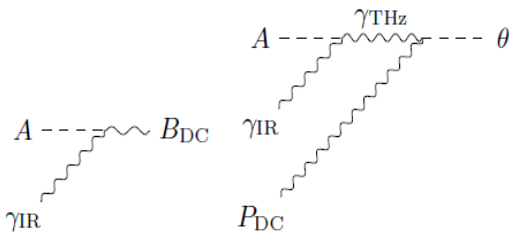


FIG. 2. **Principle of Infrared Haloscopy** Halo axion  $A$  converts infrared photon  $\gamma_{\text{IR}}$  into static magnetic field  $B_{\text{DC}}$  (left) and into terahertz photon  $\gamma_{\text{THz}}$  resonant with electromagnon  $\theta$  in ferroelectric antiferromagnet with polarization  $P_{\text{DC}}$  (right).

the symmetries  $P$ ,  $T$ ,  $CP$ , and  $CT$  [13]. The size of the shift scales with the effective four-volume  $NVT$  of the muon beam. This is our main result.

The shift in the muon spin precession frequency  $\Delta a_\mu$  due to axions in the local dark matter halo of the galaxy has roughly the right size to resolve the tension  $a_\mu(\text{Exp}) - a_\mu(\text{SM}) = (251 \pm 59) \times 10^{-11}$  between experiments (Exp) [1, 2] and standard model calculations (SM) [4, 5]. Assuming axions saturate the local halo, their energy density  $\rho_A = 0.52^{+0.12}_{-0.17} \text{ GeV}/\text{cm}^3$  follows from galactic orbital dynamics and other astrophysical constraints [14]. Similarly, the axion photon coupling strength  $|g_{A\gamma\gamma}| = (0.75 \pm 0.08) \times 10^{-10} \text{ GeV}^{-1}$  is given by observations of giant stars in globular clusters [15] assuming they had the same helium abundance in their cores when they formed as the sun did when it formed [16]. Combining these astrophysical inputs with the axion mass  $m_A = (0.508 \pm 0.004) \text{ eV}$  from cosmological considerations and symmetry arguments (See Eq. 2), we find the size of the shift  $|\Delta a_\mu| = (168 \pm 30) \times 10^{-11}$  of the muon spin precession frequency due to axions in the local dark matter halo of the galaxy roughly resolves the tension between experiment and the standard model [17].

Figure 2 shows how the axion converts infrared photons into static magnetic fields. From Eq. (2) we find the resonant wavelength  $\lambda_A = 2\pi/m_A = (2441 \pm 19) \text{ nm}$  falls in the mid-infrared. The size of the static magnetic field  $B_{\text{DC}}$  seen by an optically pumped atomic vapor, for example, scales with the infrared electric field  $E_{\text{IR}}$  [20]:

$$B_{\text{DC}} = m_A^2 g_{A\gamma\gamma} \tilde{\phi}_A(q_A) E_{\text{IR}} = \pm m_A g_{A\gamma\gamma} \sqrt{\rho_A NVT}, \quad (4)$$

where,  $N$  is the number of gas atoms,  $V$  is the beam volume within the gas cell, and  $T$  is the coherence time of the infrared light. Finding the axion resonance  $\lambda_A$  with ten parts per billion precision takes one month for a well-tuned gas cell with a tunable infrared laser locked to an external cavity[21]. Once the resonance is found, measuring  $B_{\text{DC}}$  with per cent level precision takes a day and cuts by a factor of ten the uncertainty in the shift  $|\Delta a_\mu|$  of the muon spin precession while, at the same

time, determining the sign of the shift.

Figure 2 also shows how the axion allows infrared light to excite electromagnons in ferroelectric antiferromagnets such as  $\text{BiFeO}_3$ . At room temperature the strongest electromagnon resonance in  $\text{BiFeO}_3$  lies in the terahertz regime at frequency  $\omega_\theta = 2\pi \times 0.54 \text{ THz}$ . With increasing temperature, the electromagnon softens along with the spin density wave amplitude[22]. Looking in the infrared, we expect to see the electromagnon resonance as an absorption line in transmission through a thin sample, for example, provided the light is red-detuned by  $\omega_\theta$  from the axion frequency  $\omega_A = m_A = 2\pi \times (122.9 \pm 1.0) \text{ THz}$ . Fourier transform infrared spectroscopy fixes the wavenumber of the line center with  $\Delta(1/\lambda_A) = 0.4 \text{ cm}^{-1}$  resolution. This yields the mass of the axion  $1/\lambda_A = m_A = (4100 \pm 30) \text{ cm}^{-1}$  to 100 parts per million precision[23].

We conclude that the tension between measurements of the muon magnetic moment and standard model calculations is due to axions in the local dark matter halo of the galaxy. Comparing the axion shift with the muon tension, we infer that axions saturate the local halo energy density. Weighing the axion with muon haloscopy fixes the mass to lie in the infrared at the per cent level of precision. Infrared haloscopy would improve the precision by a factor of one hundred using ferroelectric antiferromagnets and by a factor of one million using alkali vapor cells.

## ACKNOWLEDGEMENTS

We thank D. Mazura, K. Njokom, A. Virk, D. Chester, V. Subramanyan, P. H. Fisher, U. -J. Wiese, S. Watanabe, J. E. Moore, S. Haas, G. Murthy, M. Hoferichter, G. Venanzoni, A. Denig, C. Redmer, I. Logashenko, D. Nomura, H. Nguyen, K. Blaum, S. Ulmer, S. Fajfer, H. Baer, J. Mott, B. C. Regan, Y. Guo, M. Kazura, R. A. Lacey, C. M. Grayson, G. Colangelo, D. Stockinger, D. W. Hertzog, B. L. Roberts, B. Malaescu, J. M. Cline, M. Levin, B. Mueller, F. Kirk, G. Gagliardi, D. d'Enterria, G. Zanderighi, A. H. Hoang, H. Binney, A. X. El-Khadra, T. Goringe, V. Gopalan, R. D. Blandford, Z. Vallari, C. Wilkinson, J. Freericks, P. Hamilton, R. Roy, S. E. Brown, C. Jones, K. Shtengel, V. Aji, P. Kraus, R. Bruinsma, A. Kogar, C. Nayak, Z. Bern, T. Mibe, H. Wittig, T. Blum, N. Arkani-Hamed, E. Weinstein, K.-F. Liu, M. Bhaumik, M. Passera, S. Heinemeyer and J. Maldacena for insightful correspondence and discussions. This research was supported in part by the National Science Foundation under Grant No. NSF PHY-1748958.

\* nbrayali@msmu.edu

- [1] B. Abi, T. Albahri, S. Al-Kilani, D. Allspach, L. P. Alonzi *et al.* (Muon  $g - 2$  Collaboration), Measurement of the Positive Muon Anomalous Magnetic Moment to 0.46 ppm, *Phys. Rev. Lett.* **126**, 141801 (2021).
- [2] G.W. Bennett, B. Bousquet, H. N. Brown, G. Bunce, R. M. Carey *et al.* (Muon  $g - 2$  Collaboration), Final report of the muon E821 anomalous magnetic moment measurement at BNL, *Phys. Rev. D* **73**, 072003 (2006).
- [3] F. Jegerlehner, *The Anomalous Magnetic Moment of the Muon*, 2nd ed. (Springer-Verlag, 2017).
- [4] T. Aoyama, N. Asmussen, M. Benayoun, J. Bijnens, T. Blum *et al.*, The anomalous magnetic moment of the muon in the standard model, *Phys. Rep.* **887**, 1 (2020).
- [5] Sz. Borsanyi, Z. Fodor, J. N. Guenther, C. Hoelbling, S. D. Katz *et al.*, Leading hadronic contribution to the muon magnetic moment from lattice QCD, *Nature* **593**, 51 (2021).
- [6] R. D. Peccei, in *CP Violation*, edited by C. Jarlskog (World Scientific, 1989) pp. 516–517.
- [7] The axions  $A_M$  are constructed to transform under  $C$ ,  $P$ , and  $T$  as  $CA_M = A_M$ ,  $PA_M = -A_M$ , and  $TA_M = -A_M$ . To check that they do so, recall that quarks and leptons  $M_H^P$  transforms as  $CM_H^P = \overline{M}_H^{\overline{P}}$ ,  $PM_H^P = M_H^{\overline{P}}$ , and  $TM_H^P = \overline{M}_H^{\overline{P}}$ .
- [8] For anti-matter, the meaning of the parity check is reversed compared to matter:  $P = +$  indicates anti-quarks and anti-leptons which *do* feel the weak force, while  $P = -$  means the anti-matter *does not* feel it. Nevertheless, the standard model correlation between helicity  $H = L, R$  and parity check  $P = +, -$  applies in the same way to anti-matter as it does to matter:  $\overline{M}_L^-$  and  $\overline{M}_R^+$  occur in the standard model while neither  $\overline{M}_L^+$  nor  $\overline{M}_R^-$  do. See, for example, M. E. Peskin and D. V. Schroeder, *An Introduction to Quantum Field Theory* (Perseus, 1995) pp. 704–705.
- [9] J. Peebles, *Principles of Physical Cosmology* (Princeton University Press, 1993), pp. 137–138, 158–160.
- [10] D. J. Fixsen, The Temperature of the Cosmic Microwave Background, *Astrophys. J.* **707**, 916 (2009)..
- [11] N. Aghanim, Y. Akrami, M. Ashdown, J. Aumont, C. Baccigalupi *et al.* (Planck Collaboration), *Planck* 2018 Results VI. Cosmological Parameters, *A&A* **641**, A6 (2018). We use parameters from the baseline model fit to the most complete combination of available data. The results are given in *Planck* 2018 Results: Cosmological Parameter Tables, pg. 49 (May 14, 2019).
- [12] The axion  $\phi_A$  couples to photons via the term  $\mathcal{L}_{A\gamma} = \int d^3x dt g_{A\gamma\gamma} \phi_A \mathbf{E} \cdot \mathbf{B}$  in the action, where,  $\mathbf{E}$  is the electric field and  $\mathbf{B}$  is the magnetic field. We follow here the conventions of the axion theory review by R. D. Peccei [6] in which the “free” terms in the axion action take the form  $\mathcal{L}_A = \int d^3x dt [(1/2)(\partial_t \phi_A)^2 - (1/2)(\nabla \phi_A)^2 - (1/2)m_A^2 \phi_A^2]$ .
- [13] Under  $C$ ,  $PT$  and  $CPT$ , the shift  $\Delta a_\mu$ , like the axion amplitude, does not change sign.
- [14] E. I. Gates, G. Gyuk, and M. Turner, The Local Halo Density, *Astrophys. J.* **449**, L123 (1995).
- [15] A. Ayala, I. Dominguez, M. Giannotti, A. Mirizzi, and O. Straniero, Revisiting the Bound on Axion-Photon Coupling from Globular Clusters, *Phys. Rev. Lett.* **113**, 191302 (2014). They added axions to standard stellar evolution codes and found the “empirical” relation  $R = 6.26 Y - 0.41 g_{10}^2 - 0.12$  between core helium mass fraction at formation  $Y$ , axion-photon coupling  $g_{A\gamma\gamma} = g_{10} \times 10^{-10} \text{ GeV}^{-1}$ , and ratio  $R = N_{\text{HB}}/N_{\text{RGB}}$  of the number  $N_{\text{HB}}$  of giant stars in globular clusters burning helium in their core compared to the number  $N_{\text{RGB}}$  burning hydrogen in a shell around the core. Using observations of 39 globular clusters, they estimated  $R = 1.39 \pm 0.03$ .
- [16] A. M. Serenelli and S. Basu, Determining the Initial Helium Abundance of the Sun, *Astrophys. J.* **719**, 865 (2010) found  $Y_{\odot}^{\text{ini}} = 0.278 \pm 0.006$  for the abundance of helium by mass in the core of the sun at the time of formation.
- [17] For the muon beam at Fermilab E989 (FNAL) [1], the volume is  $V = 2\pi^2 R \sigma_x \sigma_y = 3.12 \times 10^4 \text{ cm}^3$ , where,  $R = 711 \text{ cm}$  is the radius of the central orbit of muons in the ring,  $\sigma_x = 1.78 \text{ cm}$  is the radial width of the beam, and  $\sigma_y = 1.25 \text{ cm}$  is the vertical width [1, 18, 19]. The average number of muons is  $N = \frac{4}{9} N_0 e^{-t_{\text{fill}}/(\gamma\tau_\mu)} \approx \frac{4}{9} \times 4340 = 1930$ , where,  $N_0 \approx 6920$  is the number of muons in the ring at the start of the fill, and  $t_{\text{fill}} \approx 30 \mu\text{sec}$  is the time it takes to fill the ring [1, 18]. The muon life-time in the haloscope rest frame is  $T = \gamma_\mu \tau_\mu = 64.4 \mu\text{sec}$ , where,  $\gamma_\mu \approx p_\mu/(m_\mu c) = 29.3$  is the muon time dilation factor,  $p_\mu = 3.10 \text{ GeV}$  is the muon momentum,  $m_\mu = 0.106 \text{ GeV}$  is the muon rest mass, and  $\tau_\mu = 2.20 \mu\text{sec}$  is the muon life-time at rest [1]. For the measurements at Brookhaven E821 (BNL) [2], we estimate  $N = 1290$ ,  $\sigma_x = 2.10 \text{ cm}$ ,  $\sigma_y = 1.53 \text{ cm}$  (J. Mott, private communication). To find the shift of muon spin precession from halo axions, we first computed  $|\Delta a_\mu(\text{FNAL})| = (169 \pm 30) \times 10^{-11}$  and  $|\Delta a_\mu(\text{BNL})| = (166 \pm 30) \times 10^{-11}$  for each experiment using Eq. (3), then we averaged these compatible yet independent results to obtain the estimated shift of the world average experimental value from the standard model calculation.
- [18] T. Albahri, A. Anastasi, K. Badgley, S. Baessler, I. Bailey *et al.* (Muon  $g - 2$  Collaboration), Beam dynamics corrections to the Run-1 measurement of the muon anomalous magnetic moment at Fermilab, *Phys. Rev. Accel. Beams* **24**, 044002 (2021).
- [19] T. Albahri, A. Anastasi, A. Anisenkov, K. Badgley, S. Baessler *et al.* (Muon  $g - 2$  Collaboration), Measurement of the anomalous precession frequency of the muon in the Fermilab Muon  $g - 2$  Experiment, *Phys. Rev. D* **103**, 072002 (2021).
- [20] The static magnetic field points along the infrared electric field for linearly polarized light. The sign of the magnetic field switches when we reverse the way the light flows through the cell.
- [21] For concreteness we take the optically pumped cesium magnetometers built by the Fribourg group to search for the electric dipole moment of the neutron: C. Abel, S. Afach, N. J. Ayres, G. Ban, G. Bison *et al.*, Optically pumped Cs magnetometers enabling a high-sensitivity search for the neutron electric dipole moment, *Phys. Rev. A* **101**, 053419 (2018). The vapor pressure of cesium  $P_{\text{Cs}} = 2.0 \times 10^{-7} \text{ Torr}$  at room temperature  $T_{\text{Cs}} = 293 \text{ K}$  yields gas number density  $n = P_{\text{Cs}}/(kT_{\text{Cs}}) = 3.8 \times 10^{10} \text{ cm}^3$ , where  $k = 1.38 \times 10^{-23} \text{ J/K}$  is the Boltzmann constant. The number of gas atoms  $N = nV_{\text{Cs}} = 4.4 \times 10^{11}$  follows from cell volume  $V_{\text{Cs}} = 4\pi R^3/3 = 11.5 \text{ cm}^3$  for radius  $R = 1.4 \text{ cm}$  of the spherical cells.

Similarly, for definiteness, we take beam parameters from the tunable external cavity diode laser TEC-500-2400-003 made by Sacher Lasertechnik Group which has power  $P = 3$  mW, line-width  $\Delta\nu = 1$  MHz, and wavelength from 2300 nm to 2500 nm that brackets the axion resonance  $\lambda_A = (2440 \pm 19)$  nm. The coherence time is  $T = 1/\Delta\nu = 1$   $\mu$ sec and the effective electric field strength is  $E_{\text{IR}} = (V/V_{\text{Cs}})\sqrt{PZ_0/(\pi w^2)} = 9.1$  V/m. Here, the beam waist  $w = 0.2$  cm sets the beam volume  $V = 2\pi w^2 R = 0.35$  cm<sup>3</sup> within the gas cell and  $Z_0 = 377$   $\Omega$  is the impedance of the vacuum. Combining the gas and laser parameters with those of the axion using Eq. (4), we find the static magnetic field  $B_{\text{DC}} = 270$  fT. For comparison, the magnetic field sensitivity of a well-tuned magnetometer is  $\sigma_B = 10.5$  fT/ $\sqrt{\text{Hz}}$ . On resonance, this gives per cent level precision after ten seconds of integration time. Finding resonance, by contrast, requires stepping through the window of width  $\sigma_{\nu_A} = c\sigma_{\lambda_A}/\lambda_A^2 = 1$  THz with step size set by the bandwidth  $\Delta\nu = 1$  MHz. Each step takes roughly 1 sec for the gas to respond. Thus, the time to find the resonance  $\sigma_{\nu_A}/\Delta\nu = 1 \times 10^6$  sec is about a month. However, the

search yields a precision for  $\lambda_A$  of  $\lambda_A\Delta\nu/c = 8 \times 10^{-9}$  that is better than ten parts per billion.

- [22] M. Bialek, A. Magrez, A. Murk, and J.-Ph. Ansermet, Spin-wave resonances in bismuth orthoferrite at high temperatures, Phys. Rev. B **97**, 054410 (2018).
- [23] The electromagnon  $\theta$  resonates when the terahertz magnetic field  $B_{\text{THz}}$  points along the spontaneous polarization  $P_{\text{DC}}$ : See Eq. (10), Fig. 2, and accompanying discussion on pg. 3 of R. de Sousa and J. E. Moore, Optical coupling to spin waves in the cycloidal multiferroic BiFeO<sub>3</sub> Phys. Rev. B **77**, 012406 (2008). The axion down-converts the red-detuned infrared photon to terahertz frequency and aligns the magnetic field  $B_{\text{THz}}$  with the infrared electric field  $E_{\text{IR}}$ . Thus, the infrared absorption occurs for light polarized along the spontaneous polarization  $P_{\text{DC}}$ . The absorption line blue-shifts towards the axion frequency  $\omega_A = m_A = 2\pi \times (122.9 \pm 1.0)$  THz with increasing temperature due to the softening of the electromagnon[22]. The basic spectral resolution  $\Delta(1/\lambda_A) = 0.4$  cm<sup>-1</sup> of the Bruker Invenio Fourier Transform infrared spectrometer fixes the axion mass with 100 parts per million precision:  $\lambda_A\Delta(1/\lambda_A) = 1 \times 10^{-4}$  for  $1/\lambda_A = m_A = (4100 \pm 30)$  cm<sup>-1</sup>.